

## Tumor cell-derived Angiopoietin-2 promotes metastasis in melanoma

Ashik Ahmed Abdul Pari<sup>1,2,\*</sup>, Mahak Singhal<sup>1,2,\*</sup>, Corinne Hübers<sup>2,3</sup>, Carolin Mogler<sup>5</sup>, Benjamin Schieb<sup>1,2</sup>,  
Anja Gamp<sup>1,2</sup>, Nicolas Gengenbacher<sup>1,2</sup>, Louise E. Reynolds<sup>6</sup>, Dorothee Terhardt<sup>2</sup>,  
Cyrill Géraud<sup>1,3,4</sup>, Jochen Utikal<sup>3,7</sup>, Markus Thomas<sup>8</sup>, Sergij Goerdt<sup>1,3</sup>,  
Kairbaan Hodivala-Dilke<sup>6</sup>, Hellmut G. Augustin<sup>1,2,9,#</sup>, Moritz Felcht<sup>1,3,#</sup>

<sup>1</sup>European Center for Angioscience (ECAS), Medical Faculty Mannheim, Heidelberg University, Mannheim, Germany; <sup>2</sup>Vascular Oncology and Metastasis, German Cancer Research Center, Heidelberg (DKFZ-ZMBH Alliance), Germany; <sup>3</sup>Department of Dermatology, Venerology und Allergology, University Medical Center Mannheim, Medical Faculty Mannheim, Heidelberg University, Mannheim, Germany; <sup>4</sup>Section of Clinical and Molecular Dermatology, Medical Faculty Mannheim, Heidelberg University, Mannheim, Germany; <sup>5</sup>Institute of Pathology, Technical University of Munich, Munich, Germany; <sup>6</sup>Center for Tumour Biology, Barts Cancer Institute, Queen Mary University of London, John Vane Science Center, London, United Kingdom; <sup>7</sup>Skin Cancer Unit, German Cancer Research Center (DKFZ), Heidelberg, Germany; <sup>8</sup>Roche Pharma Research and Early Development, Roche Innovation Center Munich, Roche Diagnostics GmbH, Penzberg, Germany; <sup>9</sup>German Cancer consortium, Heidelberg, Germany.

\*equally contributing first authors; #equally contributing last authors

**Keywords:** Angiopoietin-2, melanoma, metastasis, ROS, mitochondria, necrosis

**Running title:** Tumor cell-derived ANGPT2 promotes metastasis

**Word count:** Abstract 228; Main text: 6,489 (excluding figure legends and references)

**Conflict of interest:** Markus Thomas is an employee of Roche.

### Corresponding authors:

Dr. Moritz Felcht  
European Center for Angioscience, Medical Faculty  
Mannheim, Heidelberg University, and  
Department of Dermatology, Venerology and  
Allergy  
Theodor-Kutzer-Ufer 1-3, D-68167 Mannheim,  
Germany  
Phone: +48-621-383-2280  
Email: Moritz.felcht@umm.de

Dr. Hellmut G. Augustin  
European Center for Angioscience, Medical Faculty  
Mannheim, Heidelberg University, and  
German Cancer Research Center Heidelberg  
Im Neuenheimer Feld 280, D-69120 Heidelberg,  
Germany  
Phone: +49-6221-421500  
Email: augustin@angiogenese.de  
ORCID: 0000-0002-7173-4242

1 **Abstract**

2 The Angiopoietin (Angpt)-TIE signaling pathway controls vascular maturation and maintains the  
3 quiescent phenotype of resting vasculature. The contextual agonistic and antagonistic Tie2 ligand  
4 ANGPT2 is believed to be exclusively produced by endothelial cells, disrupting constitutive ANGPT1-TIE2  
5 signaling to destabilize the microvasculature during pathological disorders like inflammation and cancer.  
6 However, scattered reports have also portrayed tumor cells as a source of ANGPT2. Employing in situ  
7 hybridization-based detection of *ANGPT2*, we found strong tumor cell expression of *ANGPT2* in a subset  
8 of melanoma patients. Comparative analysis of biopsies revealed a higher fraction of *ANGPT2*-  
9 expressing tumor cells in metastatic versus primary sites. Tumor cell-expressed *Angpt2* was dispensable  
10 for primary tumor growth, yet in-depth analysis of primary tumors revealed enhanced intratumoral  
11 necrosis upon silencing of tumor cell *Angpt2* expression in the absence of significant immune and  
12 vascular alterations. Global transcriptional profiling of *Angpt2*-deficient tumor cells identified  
13 perturbations in redox homeostasis and an increased response to cellular oxidative stress.  
14 Ultrastructural analyses illustrated a significant increase of dysfunctional mitochondria in *Angpt2*-  
15 silenced tumor cells, thereby resulting in enhanced ROS production and downstream MAPK stress  
16 signaling. Functionally, enhanced ROS in *Angpt2*-silenced tumor cells reduced colonization potential in  
17 vitro and in vivo. Taken together, these findings uncover the hitherto unappreciated role of tumor cell-  
18 expressed ANGPT2 as an autocrine positive regulator of metastatic colonization and validate ANGPT2 as  
19 a therapeutic target for a well-defined subset of melanoma patients.

20 **Significance**

21 This study reveals that tumor cells can be a source of ANGPT2 in the tumor microenvironment and that  
22 tumor cell-derived ANGPT2 augments metastatic colonization by protecting tumor cells from oxidative  
23 stress.

24

## 25 **Introduction**

26 Melanoma patients with the occurrence of metastases at distant sites exhibit a modest 5-year survival  
27 rate of 23%, making metastasis the leading cause of melanoma-associated death (1). Recent advances in  
28 the development of novel targeted therapies against receptor tyrosine kinases (BRAF and MEK1/2) and  
29 immune checkpoints (PD-1, PD-L1, and CTLA-4) have significantly improved the overall survival and long-  
30 term disease containment for melanoma patients. Yet, only a fraction of patients with metastatic  
31 disease show long-term responses to these treatments while a majority will develop resistance towards  
32 these therapies (2,3). Furthermore, melanoma metastases can occur in the absence of any apparent  
33 primary tumor, indicating that tumor cell dissemination and metastatic seeding are early and parallel  
34 events to primary tumor progression (2,4). It is therefore necessary to unravel the underlying molecular  
35 mechanisms governing metastatic progression to rationally develop innovative strategies to treat  
36 metastatic melanoma.

37 Angiopoietin-2, a contextual agonistic and antagonistic ligand of the constitutive quiescence-maintaining  
38 endothelial ANGPT1/TIE2 signaling axis has in recent years intensely been pursued as a second-  
39 generation anti-angiogenic candidate molecule (5). Preclinically, genetic deletion of *Angpt2* resulted in a  
40 transient delay of primary tumor growth (6). Postsurgical adjuvant administration of an ANGPT2-  
41 neutralizing antibody in combination with low-dose metronomic chemotherapy restricted metastasis by  
42 quenching not only the angiogenic but also the inflammatory response of EC within the metastatic niche  
43 (7). In melanoma patients, circulating levels of ANGPT2 were associated with the progression of  
44 metastatic disease. Intriguingly, serum ANGPT2 levels were found significantly elevated in stage III/IV  
45 (metastases-bearing) but not in stage I/II (confined to the local site) melanoma patients as compared  
46 with healthy volunteers (8). These preclinical and clinical data have solidly established a crucial role of  
47 ANGPT2 during metastasis progression, particularly of melanoma metastasis, one of the earliest  
48 metastasizing tumor entities (2,4).

49 ANGPT2 is an almost endothelial cell-specifically expressed cytokine that acts in an autocrine manner to  
50 promote vascular remodeling (9). However, few scattered publications have also reported low levels of  
51 ANGPT2 expression by tumor cells of different cancer entities (8,10-12). ANGPT2 is a secreted cytokine.  
52 Immunohistochemical analysis of tumor tissue sections therefore often results in a diffuse pattern of  
53 ANGPT2 expression, making it difficult to nearly impossible to accurately determine the cellular origin of  
54 secreted ANGPT2. Therefore, definite tracing of ANGPT2 expression within the tumor microenvironment  
55 will improve our current understanding of the relative contribution of tumor cell- versus EC-secreted

56 ANGPT2 and will allow to study the functional contribution of tumor cell-secreted ANGPT2 for tumor  
57 progression and metastasis.

58 Employing *in situ* hybridization-based detection of *ANGPT2* mRNA, we unambiguously detected *ANGPT2*  
59 expression in a subset of human melanoma specimens. Indeed, a higher fraction of metastatic  
60 melanoma patients expressed *ANGPT2* in tumor cells when compared with the primary tumor and  
61 benign nevi patients. Based on these findings, we hypothesized that tumor cell-secreted ANGPT2 may  
62 contribute towards tumor progression and metastasis, possibly by affecting vascular functions or by  
63 acting in an autocrine manner on tumor cells. Detailed experimental analyses revealed that vascular or  
64 immune cell functions were not affected by tumor cell-secreted ANGPT2. Instead, tumor cell-derived  
65 ANGPT2 controlled metabolic functions of tumor cells and thereby promoted their metastatic  
66 colonization potential.

## 67 **Materials and Methods**

### 68 Cells

69 Murine MT-RET (RET) melanoma cell line was established by isolating and culturing tumor cells from a  
70 spontaneously developed tumor in MT-RET transgenic mice (13). LLC were obtained from ATCC. B16F10-  
71 Luc2 cells were purchased from Caliper life sciences, U.S.A. All human melanoma cells (SKMEL-173,  
72 SKMEL-28, C-32, WM266-4, A375, M37, SKMEL-147, and SKMEL-23) were kindly provided by J. Utikal. All  
73 cancer cells were cultured in DMEM high glucose (Gibco) supplemented with 10% FCS, 1%  
74 penicillin/streptomycin (Sigma) and 1x non-essential amino acid (Gibco). Human umbilical vein  
75 endothelial cells (HUVEC; Promocell) were cultured in Endopan-3 medium supplemented with growth  
76 factors (PAN Biotech GmbH). Mouse lung endothelial cells were acquired from Cell Biologics and were  
77 cultured in complete EC media (Cell Biologics). The cell lines used in this study were routinely tested for  
78 mycoplasma by PCR. RET and B16F10-Luc2 cells were transduced with lentiviral particles expressing  
79 shRNA constructs (Dharmacon): non-targeting (RHS4346), sh-1 *Angpt2* (V2LMM\_74366) and sh-2  
80 *Angpt2* (V2LMM\_68229). LLC cells were transduced with lentivirus to overexpress either *Angpt2* or  
81 control Plenti vector. Control or *Angpt2*-silenced RET cells were transduced with lentivirus to  
82 overexpress either *Angpt2* or control Plenti vector for rescuing *Angpt2* downregulation.

83 Antibodies

84 For immunofluorescence staining, primary [rat anti-CD31 (BD Bioscience, #550300), rabbit anti-ki67  
85 (Bethyl Laboratories, #IHC-00375), rabbit anti-desmin (Abcam, #Ab15200-1)] and secondary [anti-rat  
86 Alexa488, anti-rabbit Alexa546 (Life Technologies)] were used. Nuclei were stained with Hoechst  
87 (Sigma).

88 For Western blot analyses, primary [pERK (Cell Signaling, #4370), ERK (Santa Cruz, #sc-94), (pP38 (Cell  
89 Signaling, #9215), p38 (Cell Signaling, #9228), and  $\beta$ -actin (Santa Cruz, #sc-1616-R)] and secondary  
90 [horseradish peroxidase-conjugated antibodies (Dako)] were used. Proteins were detected with ECL  
91 (Pierce) and viewed using Amersham imager 600 (GE).

92 In vivo studies

93 Female C57BL/6N (WT) mice (8-10 weeks old) were purchased from Charles River. All mice were housed  
94 in a 12h light/dark cycle with free access to food and drinking water in specific pathogen-free animal  
95 facilities. All animal experiments were approved by the governmental (G257/18, G163/16 and G254/18  
96 from Regierungspräsidium Karlsruhe, Germany) Animal Care and Use Committees.

97 For primary tumor experiments, mice were subcutaneously injected with  $1 \times 10^6$  control or *Angpt2*-  
98 silenced RET or B16F10 cells. Two weeks post tumor implantation, mice were sacrificed and tumors and  
99 blood samples were collected for further processing. For N-acetyl-L-cysteine (NAC) (Sigma, 616-91-1)  
100 experiments, treatment was initiated on the day of tumor injection. The mice received drinking water  
101 supplemented with NAC (1g/l).

102 For LLC tumor experiments,  $1 \times 10^6$  LLC Plenti or LLC Plenti-*Angpt2* cells were inoculated subcutaneously  
103 in C57BL/6N mice. Primary tumors were surgically resected at an average size of  $150 \text{ mm}^3$ . Mice were  
104 post-resection routinely checked for the experimental endpoint criteria.

105 For experimental metastasis,  $2.5 \times 10^5$  control or *Angpt2*-silenced RET or B16F10 cells were injected in the  
106 tail vein of 8-10 weeks old female WT mice. Mice were sacrificed 2 weeks after tumor cell inoculation.  
107 Lungs were harvested and the number of metastases were counted under a stereomicroscope. For NAC  
108 treatment, the treatment was initiated one day prior to tail vein injection. The mice either received  
109 regular drinking water or drinking water supplemented with NAC (1g/l).

110 For ear tumor model,  $3 \times 10^5$  (in  $10 \mu\text{l}$ ) control or *Angpt2*-silenced RET cells were injected in the ear  
111 dermis of 8-10 weeks old WT mice. Mice were sacrificed 2 weeks after tumor cell inoculation. Cervical  
112 LN were harvested and the incidence of melanoma metastasis was evaluated under a stereo-  
113 microscope.

114 For *in vivo* lung colonization assays,  $1.5 \times 10^5$  control (red) and *Angpt2*-silenced (green) cells were co-  
115 injected intravenously in the tail vein of 8-10 weeks old female WT mice. After 2 weeks, mice were  
116 sacrificed and lungs were harvested. Images of the harvested lungs were taken using a  
117 stereomicroscope with fluorescence detection capabilities. Total RFP and GFP area in the lungs were  
118 calculated using Image J software.

#### 119 Patient samples

120 Tissue microarrays (TMA) were kindly generated by the tissue bank of the National Center for Tumor  
121 Diseases (NCT, Heidelberg, Germany) using the paraffin-embedded human tumor specimens.

#### 122 Ethical approval

123 The study was performed with archived paraffin-embedded tissue samples. The study was approved by  
124 the ethical committee of Heidelberg University (2014-835R-MA).

#### 125 Immunofluorescence and immunohistochemistry

126 Fresh tissue samples were embedded in Tissue-Tek OCT and cut into  $7\mu\text{m}$  thick cryosections for IF  
127 staining. Images were acquired using Zeiss Axio Scan and image analysis was performed with Fiji.

128 For immunohistochemistry, tissue samples were fixed in Zinc-fixative and were embedded in paraffin.  
129  $7\mu\text{m}$  sections were cut and stained with Hematoxylin and Eosin. For necrosis analysis, tumor sections  
130 were analyzed by a board-certified pathologist (C. Mogler).

131 ANGPT2 staining was performed as described earlier (14). In brief, freshly-cut TMA sections were  
132 mounted on super frost glass plates and stained with anti-ANGPT2 antibody (Santa Cruz Biotechnology)  
133 using Ultraview universal HRP multimer detection kit (Ventana, USA). Tumor sections were analyzed by  
134 C. Mogler.

#### 135 In situ hybridization

136 *In situ* hybridization was performed on TMAs using a specific probe against human *ANGPT2* and  
137 RNAscope<sup>®</sup>2.5 HD-Red kit (ACD, USA), according to the manufacturer's instructions. Afterward, the  
138 TMAs were counterstained with hematoxylin. Tumor sections were analyzed by C. Mogler.

139 Anoikis assay

140 Tumor cells were cultured under suspension condition using ultra-low attachment plates (Costar,  
141 #CLS3471-24EA) for 48h. Thereafter, the fraction of apoptotic cells was determined by FACS-based  
142 quantitation of Annexin-V (eBioscience, #88-8007-74) and FxCycle (Invitrogen, #F10347) staining.

143 Colony formation assay

144 Cells were cultured under anoikis conditions for 48h. Thereafter, 600 cells were seeded in a new 6-well  
145 plate and allowed to form colonies for 1wk. Colonies were fixed and stained with crystal violet. The  
146 number of colonies was counted manually.

147 MTT proliferation assay

148 Cells (5,000) were seeded in a 96-well plate and allowed to adhere and grow for 48h. Cellular  
149 proliferation was analyzed using cell proliferation kit (Roche, #11465007001), according to  
150 manufacturer's instruction.

151 Cell adhesion assay

152 HUVECs ( $2.5 \times 10^5$ ) were seeded in a 6-well plate to form a monolayer (24h). GFP-labeled tumor cells  
153 ( $5 \times 10^5$ ) in Opti-MEM media (Life Technologies) were seeded on the top of endothelial monolayer and  
154 allowed to adhere for 40min. Non-adherent tumor cells were washed with PBS and the count of  
155 adherent tumor cells was determined using BD Cantoll.

156 Adhesion assay

157 96-well plates were either coated with fibronectin  $10 \mu\text{g/ml}$  (Sigma) or Collagen-IV  $10 \mu\text{g/ml}$  (Sigma) at  
158  $4^\circ\text{C}$  overnight or 1h at  $37^\circ\text{C}$ . Subsequently, 30,000 tumor cells in  $100 \mu\text{l}$  Opti-MEM media were seeded in  
159 octuplicates. The cells were allowed to adhere for 40min at  $37^\circ\text{C}$ . Non-adherent cells were removed by  
160 washing the plates with PBS. The adherent cells were stained with 0.1% crystal violet solution for 10min  
161 at RT. Next, crystal violet stain was solubilized in  $100 \mu\text{l}$  of methanol and measured at 550nm in a  
162 spectrophotometer.

163 Cell migration assay

164 A CIM plate 16 (Roche Applied Science;  $8 \mu\text{m}$  pore size) was used to measure tumor cell migration on a  
165 xCELLigence system (Roche). The lower wells of the CIM plate were filled with  $160 \mu\text{l}$  full media and  $100$   
166  $\mu\text{l}$  serum free DMEM media was added on the upper wells. The plate was equilibrated for 1h at  $37^\circ\text{C}$ .  
167 After background measurement, 30,000 tumor cells in  $30 \mu\text{l}$  serum free DMEM media were added to the

168 upper chamber and the CIM plate was assembled onto the xCELLigence system and placed in the  
169 incubator at 37°C. Cell migration was assessed by monitoring changes in electric impedance every 15  
170 min for 48h. The changes in cell index over time determined the slope of the real time impedance curve.

#### 171 Cell invasion assay

172 Cell invasion was evaluated using BD BioCoat™ Matrigel™ invasion chamber (24 well plate, 8 mm pore  
173 size). After pre-hydration of invasion chambers for 1h,  $2.5 \times 10^5$  tumor cells in 500  $\mu$ L serum free DMEM  
174 were placed in the upper chamber and 750  $\mu$ L of DMEM with 10% FBS was added into the lower  
175 chamber. After 24h incubation at 37 °C, chambers were washed with PBS and fixed in Roti-Histofix (4%  
176 PFA) for 10 min. Invaded cells were stained with 0.1% crystal violet solution and counted by a bright  
177 field microscope.

#### 178 Transmigration assay

179 HUVEC ( $1 \times 10^5$ ) were plated in the top chamber of 6.5-mm/8.0- $\mu$ m 0.2% gelatin-coated Transwells  
180 (Corning) overnight. Thereafter, PKH 26-labeled tumor cells ( $1 \times 10^5$ ) were seeded in the top chamber in  
181 serum free DMEM with DMEM containing 10% FCS also in the bottom chamber. Transwells were  
182 washed 8 h later and fixed with Roti-Histofix (4% PFA) for 10 min. Transmigrated PKH 26-labelled tumor  
183 cells were counted under a fluorescence microscope.

#### 184 Immune analysis

185 Primary tumors were digested using Liberase (Roche) mix in DMEM media at 37°C for 30 min. Following  
186 ACK-lysis, single-cell suspension was equally divided, and stained for either lymphoid [CD45-PacOrange  
187 (Life Technologies, #MCD4530), CD3e-APC-e780 (eBioscience, #47-0032), CD45R(B220)-PE-Cy7  
188 (eBioscience, #25-0452), CD4-APC (BioLegend, #100412), CD8-PE (BD Pharmingen, #553033), and NK-  
189 1.1-PerCP-Cy5.5 (BioLegend, #108728)] or myeloid [CD45-PacOrange (Life Technologies, #MCD4530),  
190 CD11b-PE-Cy7 (eBioscience, #25-0112), F4/80-PE (BioLegend, #123110), Ly6C-APC-e780 (BioLegend,  
191 #128025), and Ly6G-APC (BioLegend, #127613)] panel. FxCycle-violet and 20 $\mu$ l CountBright™ Absolute  
192 Counting Beads (Thermo Fisher Scientific, #C36950) were added to exclude dead cells and to analyze the  
193 absolute cell numbers per mg of tissue, respectively. Samples were acquired on BD Aria FusionII and  
194 were analyzed with FlowJo software.

#### 195 ROS analysis

196 *In vivo*: Tumor tissues were processed into a single-cell suspension as described above and incubated  
197 with CellRox-Deep Red (Thermo Scientific, #C10422) for 30min at 37°C in full media (FM). Cellular ROS



198 was measured by quantifying the mean fluorescent intensity (MFI) of CellROX dye in FxCycle<sup>-</sup>CD45<sup>-</sup>CD31<sup>-</sup>  
199 Ter119<sup>-</sup>GFP<sup>+</sup> tumor cells using BD Cantoll.

200 *In vitro*: Cells were cultured in either FM or serum-starved media and kept under anoikis conditions for  
201 48h. Thereafter, cells were stained with CellRox-Deep Red as described above. Live cells were analyzed  
202 for MFI of CellRox dye.

### 203 ELISA

204 ANGPT2 protein levels in the cell culture supernatant and serum were determined using either mouse  
205 ANGPT2 (R&D, #MANG20) or human ANGPT2 (R&D, #DANG20) ELISA kits, according to the  
206 manufacturer's protocol.

207

### 208 Gene expression analysis

209 Total RNA, isolated by homogenizing tumor tissue, was used for reverse transcription using QuantiTect  
210 Reverse Transcription Kit (Qiagen) according to the manufacturer's instructions. cDNA was used for RT-  
211 qPCR using TaqMan Fast Advanced Mastermix and TaqMan probes [*TEK* (Hs00945146\_m1); *ANGPT2*  
212 (Hs01048042\_m1); *ACTB* (Hs01060665\_g1); *Angpt2* (Mm00545822\_m1); *Hmox1* (Mm00516005\_m1);  
213 *Actb* (Mm00607939-s1); *Mki67* (Mm01278617\_m1); *Fis1* (Mm00481580\_01); *Dnm1l*  
214 (Mm01342903\_m1); Applied Biosystems] on a LightCycler-480 (Roche) system. Gene expression was  
215 calculated by  $\Delta\Delta C_t$  method.

### 216 Microarray analysis

217 Microarrays were conducted by the DKFZ Genomics and Proteomics core facility. In brief, total RNA from  
218 tumor cells was used to generate libraries which were hybridized on Affymetrix GeneChip™ Mouse Gene  
219 2.0 ST arrays (Affymetrix). Microarray data were normalized using Affymetrix Expression Console  
220 software and differential gene expression was calculated using Affymetrix Transcriptome Analysis  
221 Console. Gene Set Enrichment Analysis (GSEA) and Ingenuity Pathway Analysis (IPA) were performed to  
222 annotate the differentially regulated molecular pathways. The microarray data with the description are  
223 deposited under GEO accession no. GSE146320.

### 224 Seahorse analysis

225 Mitochondrial function of tumor cells was measured using Mito stress test in XF96 extracellular flux  
226 analyzer (Seahorse Bioscience) according to the manufacturer's instruction. Tumor cells (10,000 per

227 well) were seeded in a 96-well Seahorse cell culture plate and incubated overnight. Next day, the cells  
228 were shifted to 1% O<sub>2</sub> condition (Hypoxia) for 6h at 37°C. After hypoxia treatment, the cells were  
229 washed twice and the media was replaced with DMEM sea horse media (Seahorse Bioscience)  
230 containing 1mM pyruvate (Sigma), 2mM glutamine (Gibco), and 10mM glucose (Sigma). Next, the plate  
231 containing the cells was kept in non-humidified 37°C incubator 1h prior to start of the experiment.  
232 Oxygen consumption rate (OCR) was measured at the basal level and after addition of the following  
233 compounds: oligomycin (Sigma, 0.5 μM), FCCP, (Sigma, 0.25 μM) and rotenone (Sigma, 0.5 μM). The  
234 data were analyzed using the wave software (Seahorse Bioscience) according to the manufacturer's  
235 instructions. Proton leak was calculated by subtracting non-mitochondrial respiration from minimum  
236 rate measurement after oligomycin injection.

#### 237 TCGA analysis

238 Spearman correlation analysis of TCGA gene expression datasets from Skin Cutaneous Melanoma  
239 (SKCM) samples was performed using GEPIA web portal.

#### 240 Human Protein Atlas analysis

241 Kaplan-Meier graphs were plotted from the survival information of melanoma patients extracted from  
242 Human Protein Atlas database.

#### 243 Transmission electron microscopy

244 Transmission electron microscopy was performed in the DKFZ electron microscopy core facility. Tumor  
245 cells were grown on punched Aklar (EMS, Germany) under serum-starvation and hypoxic conditions for  
246 24h. Thereafter, cells were fixed in buffered aldehyde (4% formaldehyde, 2% glutaraldehyde, 1mM  
247 MgCl<sub>2</sub>, 1mM CaCl<sub>2</sub> in 100mM Ca-cacodylate, pH 7.2), post-fixed in aqueous 1% osmium tetroxide  
248 followed by en-block staining in 1% ethanolic (75%)-uranylacetate. Following dehydration in graded  
249 steps of ethanol, the adherent cells got flat-embedded in epoxide (Glycidether, NMA, DDSA: Serva,  
250 Germany). Ultrathin 50nm sections were cut and contrast-stained with lead-citrate and uranylacetate.  
251 The sections were imaged with a Zeiss EM910 at 120kV (Carl Zeiss, Germany) and micrographs were  
252 taken with a CCD-Camera (TRS, Germany). Mitochondria with disrupted cristae structure were counted  
253 and quantification was done manually without prior-knowledge of biological groups.

#### 254 Statistical analysis

255 All data are expressed as mean with error bars depicted as SD or SEM (indicated in figure legends). n  
256 represents the number of independent experiments in case of *in vitro* experiments and the number of

257 mice for *in vivo* experiments. Statistical analyses were performed using GraphPad Prism 6. Comparisons  
258 between two groups were made using two-tailed unpaired Student's t-test, non-parametric Mann  
259 Whitney U-test, or paired t-test. A p-value of less than 0.05 was considered statistically significant.

## 260 **Results**

### 261 Tumor cells in melanoma patients express ANGPT2

262 To investigate the abundance and cellular source of ANGPT2 in melanoma patients, we performed  
263 immunohistochemical staining of ANGPT2 in primary tumors and metastatic tissue biopsies. In line with  
264 previous publications, a substantial fraction (26/68) of melanoma biopsies expressed high levels of  
265 ANGPT2 (Fig. 1A, Supplementary Fig. S1A, B). A closer look at the stained tissue micro-arrays (TMA)  
266 revealed two different staining patterns – one in which ANGPT2 was confined to blood vessels (Fig. 1A,  
267 upper image) and a second with more diffuse pleiotropic presence of ANGPT2 (Fig. 1A, lower image),  
268 thereby hinting to different cellular sources of secreted ANGPT2. To conclusively determine the source  
269 of ANGPT2 in tumor tissues, we employed *in situ* hybridization (ISH)-based staining of *ANGPT2* mRNA in  
270 an independent melanoma TMA. Indeed, ISH analysis demonstrated that tumor cells, in addition to EC,  
271 expressed *ANGPT2* in a subset of melanoma biopsies (Fig. 1B). Forty-seven of 133 analyzed samples  
272 (using ISH) had detectable *ANGPT2* expression (Supplementary Fig. S1A) and 23 of these showed  
273 *ANGPT2* expression in tumor cells. Since serum levels of ANGPT2 had been shown to correlate with  
274 prognosis of melanoma patients, we assessed whether tumor cell-expressed *ANGPT2* could serve as a  
275 predictive biomarker for melanoma progression (6). Indeed, a higher fraction (28.2%) of metastatic  
276 melanoma patient biopsies had *ANGPT2* expression in tumor cells when compared with primary tumor  
277 and benign nevi samples (Fig. 1C). This implied that increased ANGPT2 expression in tumor cells was  
278 associated with metastatic progression. Moreover, analysis of Human Protein Atlas datasets revealed an  
279 inverse correlation between *ANGPT2* expression levels and overall survival of melanoma patients  
280 (Supplementary Fig. S1C). Taken together, human melanoma cells express and secrete ANGPT2 and  
281 *ANGPT2* expression is a prognostic marker for metastatic melanoma.

### 282 *Angpt2* silencing in tumor cells enhances intratumoral necrosis

283 To examine the functional role of tumor cell-derived ANGPT2, a set of human and mouse melanoma cell  
284 lines was screened for *ANGPT2* gene expression, wherein 5/8 human (Supplementary Fig. S1D) and 2/2  
285 mouse (Fig. 1D) melanoma cell lines were found positive for *ANGPT2* expression. Side-by-side  
286 comparison of *ANGPT2* expression levels in tumor cells with the corresponding mouse or human EC

287 showed that mouse tumor cells had endogenous *Angpt2* levels similar to murine lung EC, whereas  
288 human melanoma cells expressed *ANGPT2* to a lower extent compared with HUVEC. Despite significant  
289 *Angpt2* expression, both murine melanoma cell lines lacked detectable expression of the cognate  
290 signaling receptor Tie2 (*Tek*; Fig. 1D). In the case of human tumor cells, 8/8 cell lines displayed low but  
291 detectable levels of *TEK* (Supplementary Fig. S1E). Based on endogenous *ANGPT2* expression, we chose  
292 3 cell lines, including 2 murine (RET, B16F10) and 1 human (SKMEL-28), with relatively higher *ANGPT2*  
293 expression to determine whether these cell lines secreted *ANGPT2*. Indeed, all three tested cell lines  
294 secreted *ANGPT2* with conditioned media concentrations ranging from 0.44 ng/ml in SKMEL-28 to 2.4  
295 ng/ml and 3.8 ng/ml in B16F10 and RET cell lines, respectively (Fig. 1E, Supplementary Fig. S1F). Tumor  
296 cell-secreted *ANGPT2* may act either in a paracrine manner on stromal cells (EC, Tie2<sup>+</sup> macrophages) or  
297 in an autocrine manner on melanoma cells. Considering that both, RET and B16F10 cells secreted much  
298 higher amounts of *ANGPT2* as compared with SKMEL-28 cells, we selected these two melanoma cells for  
299 further experimentation. Additionally, the syngeneic status of RET and B16F10 cells allowed us to  
300 perform all *in vivo* experiments in immunocompetent mice, thereby assessing the impact of tumor cell-  
301 derived *ANGPT2* on all stromal components of the tumor microenvironment.

302 To study the functional role of tumor cell-derived *ANGPT2* during tumor progression, shRNA mediated  
303 knockdown of *Angpt2* was performed in RET and B16F10 cells. Effective silencing of *Angpt2*, both at the  
304 mRNA and protein levels, was achieved *in vitro* using two independent shRNAs (sh-1 and sh-2; Fig. 1E,  
305 Supplementary Fig. S2A). Reduced expression of *Angpt2* did not affect the proliferation of tumor cells in  
306 an *in vitro* MTT-based assay (Supplementary Fig. S2B). Next, to examine whether the lack of tumor cell-  
307 derived *ANGPT2* affected primary tumor growth,  $1 \times 10^6$  control (non-targeting) or *Angpt2*-silenced  
308 tumor cells (RET and B16F10) were implanted subcutaneously in C57BL/6N mice. Mice were sacrificed  
309 14 days after tumor inoculation and primary tumor weights were measured (Fig. 2A, Supplementary Fig.  
310 S3A, B). QPCR analysis of whole tumors verified a significant downregulation of *Angpt2* in both  
311 experimental models (Fig. 2B, Supplementary Fig. S3C). Further, ELISA-based quantitation confirmed a  
312 significant reduction of *ANGPT2* protein in *Angpt2*-depleted primary tumors (Supplementary Fig. S3D).  
313 In line with our previous *in vitro* observations, no significant difference was observed in primary tumor  
314 growth between the non-targeting control and *Angpt2*-silenced tumors. In-depth histological analysis of  
315 tumor tissue sections revealed that *Angpt2*-silenced tumors had higher intratumoral necrosis in both  
316 tumor models as compared with control tumors (Fig. 2C, Supplementary Fig. S3E, F). Further, qPCR  
317 (Supplementary Fig. S3G, H) and immunofluorescence (IF) (Fig. 2D, Supplementary Fig. S3I, J) analyses of  
318 the proliferation marker Ki67 did not show differences between control and *Angpt2*-silenced primary

319 tumors, indicating that enhanced necrosis did not result in a reduction of tumor cell proliferation.  
320 Reintroduction of *Angpt2* expression in *Angpt2*-depleted tumor cells abolished the intratumoral necrosis  
321 associated with the loss of *Angpt2* in tumor cells (Fig. 2E, F). Thus, enhanced necrosis in *Angpt2*-  
322 depleted tumors is resulting specifically from the lack of *Angpt2* and was not due to potential shRNA off-  
323 target effects. Overall, the data suggested that tumor cell-derived ANGPT2 was largely dispensable for  
324 primary tumor growth and suppressed intratumoral necrosis.

#### 325 Tumor cell-derived ANGPT2 does not alter tumor stroma

326 EC-derived ANGPT2 acts autocrine on blood vessels, thereby priming otherwise, quiescent EC for  
327 sprouting angiogenesis (9). We therefore hypothesized that tumor cell-secreted ANGPT2 might act  
328 similarly to facilitate tumor neoangiogenesis and potentially defunct neoangiogenesis might have  
329 resulted in the increased intratumoral necrosis as observed in *Angpt2*-silenced tumors. To this end, the  
330 tumor vasculature was analyzed in control and *Angpt2*-silenced primary tumor samples. The IF-based  
331 vascular analysis revealed that the absence of tumor cell-secreted *Angpt2* affected neither microvessel  
332 density nor pericyte coverage in both melanoma models (Supplementary Fig. S4A-D). Thus, the data  
333 excluded apparent effects of cancer cell-derived ANGPT2 on the tumor vasculature, possibly suggesting  
334 that stromal-derived ANGPT2 was sufficient to sustain tumor neoangiogenesis.

335 Recently, ANGPT/TIE signaling has been shown to regulate tumor immune surveillance. Mechanistically,  
336 dual-inhibition of ANGPT2 and VEGFA resulted in increased tumor necrosis and enhanced antigen  
337 presentation by intratumoral phagocytes which eventually led to an increase in infiltration of CD8+  
338 cytotoxic T-cells (15). This prompted us to test whether the increased necrosis in *Angpt2*-silenced  
339 tumors might be attributed to alterations in immune cell infiltration. FACS-based immune phenotyping  
340 revealed no significant differences in either lymphoid (Fig. 3A, Supplementary Fig. S4E) or myeloid (Fig.  
341 3B, Supplementary Fig. S4F) cell populations when comparing non-targeting control and *Angpt2*-silenced  
342 tumors. Therefore, the data ruled out a possible contribution of immune cells in enhancing tumor  
343 necrosis in *Angpt2*-silenced tumors.

#### 344 ANGPT2 affects intracellular oxidative stress signaling

345 With no detectable alterations in the vascular architecture and immune cell infiltration, we next  
346 investigated possible autocrine effects of *Angpt2* silencing on tumor cells. To this end, global  
347 transcriptomic profiling of *in vitro*-cultured non-targeting control and *Angpt2*-silenced tumor cells was  
348 performed to trace changes of transcriptional gene signatures. Gene set enrichment analysis (GSEA)  
349 revealed that *Angpt2* knockdown in tumor cells perturbed cellular redox homeostasis as indicated by

350 the enrichment of gene sets involved in the biosynthesis of reactive oxygen species (ROS) and  
351 subsequent cell death in response to oxidative stress (Fig. 4A). Additionally, pathways regulating  
352 metastasis, the antioxidant stress response and mitochondrial function were found regulated in *Angpt2*-  
353 silenced tumor cells (Fig. 4A, Supplementary Fig. S5A, B). Indeed, the NFE2L2 (NRF2) signaling pathway,  
354 which underlines one of the major cellular defense mechanisms to resolve cellular oxidative stress, was  
355 found downregulated in *Angpt2*-silenced tumor cells (Fig. 4A) (16). Therefore, enhanced production of  
356 ROS together with crumbling cellular antioxidative defense mechanisms may have led to elevated levels  
357 of intracellular oxidative stress in the absence of *Angpt2* expression. Indeed, *in silico* analysis of TCGA  
358 human skin cutaneous melanoma (SKCM) dataset revealed a positive correlation between *ANGPT2* and  
359 *NFE2L2* expression (Fig. 4B), substantiating our findings from *Angpt2*-deficient murine melanoma cells.  
360 Furthermore, the expression of *HMOX1*, a key downstream enzyme in the NRF2 signaling cascade and  
361 scavenger for cellular ROS (16), also positively correlated with *ANGPT2* in the TCGA-SKCM dataset (Fig.  
362 4B).

363 To confirm these *in vitro* findings *in vivo*, we assessed the expression of *Hmox1* in control and *Angpt2*-  
364 silenced tumors. Corroborating our earlier findings, *Angpt2*-silenced tumors manifested lower  
365 expression of *Hmox1* as compared with control tumors (Fig 4C, Supplementary Fig. S6A). To examine  
366 whether the reduced expression of *Hmox1* resulted in perturbed redox homeostasis, intracellular ROS  
367 levels were measured in tumor cells isolated from primary tumors. Increased ROS levels were detected  
368 in *Angpt2*-silenced as compared with control tumor cells, thereby implying a malfunctioning redox  
369 homeostasis (Fig. 4D, Supplementary Fig. S6B). Interestingly, *in vitro*-cultured *Angpt2*-deficient tumor  
370 cells did not show any change in ROS production under normal culture conditions as compared with  
371 control cells (Supplementary Fig. S6C). Yet, under serum starvation, *Angpt2* silencing led to a significant  
372 increase in intracellular biosynthesis of ROS (Supplementary Fig. S6C), possibly capturing the nutrition-  
373 deprived *in vivo* conditions. Further, restoring *Angpt2* expression in *Angpt2*-silenced tumor cells rescued  
374 the ROS levels to homeostatic conditions (Supplementary Fig. S6D).

375 Enhanced ROS production has previously been reported to induce necrosis (5). This led us to  
376 hypothesize that increased ROS levels in *Angpt2*-depleted tumors could have resulted in the observed  
377 necrosis phenotype. To further experimentally validate this hypothesis *in vivo*, mice implanted with  
378 either control or *Angpt2*-silenced tumor cells were administered ROS inhibitor N-acetyl-L-cysteine (NAC)  
379 in drinking water (Supplementary Fig. S6E). NAC treatment abrogated the previously-observed increase  
380 in intratumoral necrosis in *Angpt2*-depleted as compared with non-targeting control tumors (Fig. 2C,

381 Supplementary Fig. S6F, G). These data indicated that enhanced intracellular ROS in *Angpt2*-depleted  
382 tumors may have resulted in increased intratumoral necrosis.

383 The rapid growth of a primary tumor is often accompanied by nutrient deprivation and induction of  
384 hypoxia in the center of tumor tissue (17). Such a hostile environment can have detrimental effects on  
385 mitochondrial function in tumor cells. Subsequently, mitochondria lose their morphology and cristae  
386 structure, essential determinants of their physiological function, and begin to produce high levels of ROS  
387 (18,19). To investigate whether mitochondrial morphology was altered in *Angpt2*-silenced tumor cells,  
388 we performed ultrastructural analyses of tumor cells cultured under different conditions (hypoxia and  
389 serum starvation) by transmission electron microscopy. Under normoxic conditions, no significant  
390 differences in the mitochondrial structure was observed upon *Angpt2* knockdown (Supplementary Fig.  
391 S7A, B). Yet, under hypoxic conditions, mitochondrial morphology was highly irregular with near-  
392 complete loss of cristae structure in *Angpt2*-silenced as compared with control tumor cells (Fig. 4E).  
393 Concurrently, the number of fragmented mitochondria per cell was significantly increased (Fig. 4F).  
394 Expression analysis of genes involved in mitochondrial dynamics showed a reduced expression of Drp1  
395 (*Dnm1l*) and *Fis1* in *Angpt2*-depleted primary tumors (Supplementary Fig. S7C, D). DRP1 and FIS1 are  
396 required for maintaining mitochondrial integrity, therefore their downregulation highlights perturbation  
397 in mitochondrial function in the absence of *Angpt2* expression (20,21).

398 To determine an unambiguous readout of mitochondrial function, a Seahorse Mito Stress experiment  
399 was conducted to determine the mitochondrial bioenergetic profile of tumor cells. Proton leak, a key  
400 parameter in a Seahorse experiment, represents the oxygen consumption rate (OCR) associated with all  
401 ion movement across the inner mitochondrial membrane during ATP synthesis (22). Indeed, the loss of  
402 ANGPT2 resulted in a significant reduction of proton leak in tumor cells, thereby confirming diminished  
403 mitochondrial function (Fig. 4G). Furthermore, elevated ROS levels, due to curtailed mitochondrial  
404 function, have been shown to activate MAPK stress signaling (23). Concomitantly, increased  
405 phosphorylation levels of ERK and P38, key components of the MAPK pathway, were observed in  
406 *Angpt2*-silenced primary tumors when compared with control tumors (Fig. 4H, Supplementary Fig. S7E).  
407 Overall, the data established an important role of tumor cell-expressed *Angpt2* in maintaining  
408 mitochondrial function and redox homeostasis.

#### 409 Tumor cell-expressed *Angpt2* facilitates metastasis

410 To investigate if *Angpt2* deficiency affected the metastatic potential of melanoma cells, tumor cells were  
411 intravenously injected to initiate an experimental metastasis assay. Loss of tumor cell-expressed *Angpt2*

412 resulted in a significant reduction in lung metastases in both melanoma models (Fig. 5A, B,  
413 Supplementary Fig. S8A, B). To circumvent the substantial heterogeneity of the experimental metastasis  
414 assay, we performed an indexed analysis by co-injecting RFP-labeled control and GFP-labeled *Angpt2*-  
415 silenced cells in mice and measured the composition of lung metastases *ex vivo* 14 days after  
416 intravenous injection. Unambiguously, *Angpt2*-silenced tumor cells exhibited reduced metastatic  
417 potential as compared with control cells (Fig. 5C, D, Supplementary Fig. S8C, D). Moreover, rescuing  
418 *Angpt2* expression in *Angpt2*-depleted cells reversed the observed decline in metastasis (Fig. 5E, F),  
419 thereby indicating that reduction of metastasis was due to the loss of *Angpt2*. Next, we employed a  
420 cervical LN metastasis model in which intradermally-inject tumor cells in the ear colonize the draining  
421 LN. Similar to the lung experimental metastasis assay, depletion of tumor cell-*Angpt2* reduced the  
422 incidence of cervical LN metastasis (Fig. 5G, H). To substantiate the findings in a spontaneous metastasis  
423 model, we utilized the LLC post-surgical model in which lung metastases develop after surgical removal  
424 of the primary tumor (Supplementary Fig. S8E). Indeed, there was a significant decrease in post-surgical  
425 survival of mice implanted with *Angpt2*-overexpressing as compared with control LLC cells  
426 (Supplementary Fig. S8F, G).

427 Based on the above findings, we hypothesized that the observed decrease in metastatic capability of  
428 *Angpt2*-depleted cells could be due to enhanced oxidative stress. To experimentally investigate this  
429 hypothesis, mice injected intravenously with either control or *Angpt2*-silenced RET cells were treated  
430 with ROS scavenger NAC. In line with the primary tumor data, administration of NAC in mice injected  
431 with *Angpt2*-deleted tumor cells rescued the observed reduction of metastasis upon loss of *Angpt2* in  
432 tumor cells (Fig. 6A-C). Collectively, these experiments underline tumor cell-expressed *Angpt2* as a  
433 crucial regulator of their metastatic capability, primarily by altering intracellular ROS and subsequent  
434 cellular oxidative stress.

435 Next, we performed a set of experiments to mechanistically decipher the role of tumor cell-expressed  
436 *Angpt2* on different steps of the metastatic cascade experienced by the tumor cells in an experimental  
437 metastasis model. Examining the role of migration, anoikis-induced tumor cell death, tumor cell  
438 adhesion to EC and to ECM depicted no significant differences between control and *Angpt2*-silenced  
439 tumor cells, suggesting that tumor cell-expressed *Angpt2* did not impact early steps of the metastatic  
440 cascade (Supplementary Fig. S9A-H). Subsequently, we assessed whether tumor cell-derived ANGPT2  
441 was required for tumor cell invasion and transmigration. Downregulation of *Angpt2* hindered the  
442 capability of tumor cells to invade through the basement membrane and transmigrate across the



443 endothelial barrier (Supplementary Fig. S10A-H). Further, we evaluated whether tumor cell-expressed  
444 *Angpt2* affected the ability of tumor cells to colonize the metastatic site. To simulate *in vivo* conditions  
445 for colonization, tumor cells were treated under anoikis conditions for 48h and a colony formation assay  
446 was initiated thereafter. Lack of *Angpt2* decreased the colonization potential of tumor cells as indicated  
447 by sharp reduction in the number of colonies (Supplementary Fig. S11A-D). Concordantly,  
448 overexpressing *Angpt2* in *Angpt2*-depleted tumor cells recovered the colonizing capability of the tumor  
449 cells (Supplementary Fig. S11E,F). These findings demonstrate that tumor cell-expressed *Angpt2*  
450 promoted metastasis by facilitating the colonization process.

## 451 **Discussion**

452 The incidence of melanoma has been steadily rising during the last 50 years. While the 5-year survival  
453 rate for patients with locally-contained (stage I) melanoma is 98%, distant metastasis is often life-  
454 threatening with a modest survival rate of 23% (1). This can largely be attributed to early metastatic  
455 spread and non-reliable detection of primary lesions. It is estimated that approximately 10% of  
456 melanomas go undetected with the current diagnostic methods (4). Previously, we have established  
457 serum ANGPT2 as a reliable biomarker for melanoma progression, especially to distinguish stage III/IV  
458 from primary melanomas (8). Indeed, patients with distant organ metastasis (stage IV) had on average  
459 4-fold higher levels of serum ANGPT2 when compared with patients with lymph-node (LN)-restricted  
460 tumors (stage III). Intriguingly, immunoperoxidase-based analysis of advanced-stage tumors revealed a  
461 weak but consistent expression of ANGPT2 in tumor cells. These data raised the question of relative  
462 abundance and functional role of tumor cell-expressed ANGPT2 during melanoma metastasis.

463 Employing a wide array of clinical and preclinical analysis, the present study demonstrates that (1)  
464 tumor cells serve as a source of ANGPT2 in a fraction of melanoma patients; (2) loss of endogenous  
465 *Angpt2* expression in tumor cells neither affects primary tumor growth, nor does it influence tumor  
466 angiogenesis and the immune landscape, but rather results in enhanced intratumoral necrosis; (3)  
467 *Angpt2* silencing in tumor cells perturbed cellular redox homeostasis by augmenting mitochondrial  
468 dysfunction; and (4) *Angpt2* silencing in melanoma cells profoundly suppressed lung metastases due to  
469 enhanced ROS production, which led to reduction in colonization potential of *Angpt2*-silenced tumor

470 cells. Together, these data reveal novel functions of cancer cell-derived ANGPT2 during melanoma  
471 progression.

472 Following the clinical approval of VEGF/VEGFR-targeting drugs, ANGPT/TIE signaling was pursued as  
473 second generation angiogenesis-regulating vascular tyrosine kinase system for its ability to  
474 synergistically enhance the efficacy of approved anti-angiogenic therapies (5). Similar to VEGF, ANGPT2  
475 was found upregulated in both primary tumor tissues and the circulation of multiple cancer entities. Yet,  
476 whereas VEGF is primarily secreted by the tumor cells, ANGPT2 is almost exclusively produced by tumor-  
477 associated EC (24). Yet, some melanoma biopsies from patients with advanced disease manifested a  
478 rather diffuse staining of ANGPT2 compared with the confined blood vessel-restricted staining in other  
479 tumors. Likewise, several cultured human melanoma cell lines have been reported to express ANGPT2  
480 (8). Here, employing *in situ* hybridization, we unambiguously traced the cellular source of ANGPT2 in  
481 human tissue microarrays. Clearly, tumor cells in a subset of human melanomas expressed and secreted  
482 ANGPT2. However, unlike the granular pattern of ANGPT2 staining observed in EC due to its localization  
483 in Weibel-Palade bodies, ANGPT2 staining in TMA sections had a uniform cytoplasmic localization  
484 pattern in tumor cells (25). This suggests that ANGPT2 in tumor cells may not be stored and rapidly  
485 released upon stimulation.

486 Evaluation of ANGPT2 expression in melanoma patient samples demonstrated that the fraction of  
487 patients with tumor cell-expressed ANGPT2 was much higher in the metastatic specimens as compared  
488 with either nevus or primary melanomas, thereby suggesting a crucial role of tumor cell-expressed  
489 ANGPT2 for melanoma metastasis.

490 Host-derived ANGPT2 has been shown to affect early stages of primary tumor growth but is largely  
491 dispensable for the growth of established tumors (6). Concurrently, administration of ANGPT2-  
492 neutralizing antibody delayed primary tumor growth of xenografted human cells (26). Mechanistically,  
493 ANGPT2-blockade restricted EC proliferation and enhanced pericyte coverage for improved perfusion  
494 properties. Apart from the proangiogenic function of ANGPT2, ectopic overexpression of ANGPT2 in  
495 human breast cancer cells has been described to act autocrine, thereby promoting cellular invasiveness  
496 to facilitate distant metastasis (27). Likewise, ANGPT2 overexpression in glioma cells induced tumor cell  
497 invasion in an MMP2-dependent manner (28). Thus, previous publications have hinted towards an  
498 autocrine, angiogenesis-independent role of cancer cell-expressed ANGPT2 during tumor progression.  
499 However, the previous studies have relied on exogenous overexpression of ANGPT2, which often tends  
500 to flood the cellular environment with non-physiological amounts of protein, thereby interfering with

501 their normal cellular function (29). To circumvent this artificial gain-of-function approach, we utilized  
502 two mouse melanoma cell lines, RET and B16F10, with high endogenous expression of *Angpt2*, similar to  
503 mouse lung EC. ShRNA-mediated knockdown of *Angpt2* in tumor cells did not alter primary tumor  
504 growth. Further, tumor cell-specific silencing of *Angpt2* neither affected tumor vasculature nor the  
505 immune milieu. The loss of tumor cell-secreted ANGPT2 was possibly compensated by the host  
506 endothelium. Surprisingly though, primary tumors arising from *Angpt2*-silenced melanoma cells  
507 displayed increased intratumoral necrosis when compared with non-targeting control tumors, thereby  
508 emphasizing a protective role of tumor cell-expressed *Angpt2* during primary tumor growth.

509 Comparative transcriptomic analysis of control and *Angpt2*-silenced tumor cells identified perturbations  
510 in intracellular redox homeostasis. *Angpt2* deficiency in tumor cells positively correlated with gene sets  
511 involved in ROS biosynthesis and subsequent cell death due to oxidative stress. In turn, lack of ANGPT2  
512 led to downregulation of NFE2L2 targets. NFE2L2 (Nrf2), an upstream transcriptional regulator for  
513 multiple ROS-scavenging enzymes, protects a cell from oxidative damage (16). Indeed, tumors arising  
514 from *Angpt2*-silenced melanoma cells showed reduced expression of *Hmox1* (a downstream effector of  
515 NFE2L2), and recorded higher levels of intracellular ROS as compared with control tumors. Moreover,  
516 antioxidant treatment of mice bearing *Angpt2*-depleted primary tumors resulted in reduction of overall  
517 intratumoral necrosis. This implied that intracellular ROS generated after *Angpt2*-silencing in tumor cells  
518 drives necrosis in primary tumors. Correspondingly, analysis of TCGA-SKCM data set revealed a positive  
519 correlation between *ANGPT2* and *NFE2L2/HMOX1* expression, further bolstering a crucial role of tumor  
520 cell-expressed *ANGPT2* in minimizing stress-induced oxidative damage.

521 Unrestricted growth of primary tumors results in a hypoxic and nutrient-deprived core (30). In a hypoxic  
522 microenvironment, tumor cells adapt their mitochondrial function to slow down oxidative  
523 phosphorylation and hyperactivate NRF2 pathway to lower intracellular levels of ROS (19). Any  
524 imbalance in these protective mechanisms may result in the accumulation of ROS and sustained  
525 oxidative damage. Melanoma cells quickly adapt to the hypoxic conditions as they did not display major  
526 alterations in the mitochondrial ultrastructure. Nevertheless, in the absence of *Angpt2* expression,  
527 melanoma cells witnessed a higher fraction of dysfunctional mitochondria and subsequent reduction in  
528 energy production. Hence, enhanced expression of *Angpt2* in melanoma tumor cells acts as a defense  
529 mechanism against cellular stress. These findings are in line with a recent publication highlighting the  
530 protective role of ANGPT2 on hepatocellular cancer cell line HepG2 under Doxorubin-induced cytotoxic  
531 stress by reducing ROS production and preserving mitochondrial function (31).

532 Despite no apparent effects on primary tumor growth, *Angpt2*-silenced melanoma cells led to reduced  
533 lung metastasis in experimental metastasis assays. Mechanistically, *Angpt2* silencing restricted the  
534 efficacy of metastatic colony formation of melanoma cells. Likewise, ectopic expression of ANGPT2 in  
535 PDAC xenografts was reported to display an enhanced rate of lymphatic metastasis (32). Successful  
536 colonization at a distant organ site requires a single-seeded tumor cell to survive in a hostile  
537 microenvironment and to overcome a variety of extracellular and intracellular stresses. Our molecular  
538 data underline an important role of tumor cell-expressed *Angpt2* in maintaining intracellular oxidative  
539 balance and preserving mitochondrial function. Notably, ROS scavenger NAC effectively reinstated the  
540 metastatic capacity of *Angpt2*-depleted tumor cells. Thus, tumor cell-*Angpt2* protects melanoma cells  
541 from oxidative stress and ensures their survival during the metastasis process. These mechanistic  
542 findings explain why a higher fraction of metastatic melanoma biopsies displayed tumor cell-expressed  
543 ANGPT2.

544 In summary, the present study, by establishing spatial distribution of ANGPT2 expression in metastatic  
545 melanoma, has revealed the cellular source of ANGPT2 in melanoma and shed light on the molecular  
546 and functional contribution of tumor cell-expressed *Angpt2* during metastasis. The findings expand the  
547 hitherto endotheliocentric view of angiopoietin functions and validate ANGPT2 as a therapeutic target  
548 for a well-defined subset of melanoma patients.

#### 549 **Acknowledgements**

550 We would like to thank Dr. Karsten Richter and Dr. Michelle Neßling from the DKFZ electron microscopy  
551 core facility for their assistance in acquiring electron microscopy images. We would like to thank Dr.  
552 Suzana Vega Haring from Roche for performing the ANGPT2 staining. We would like to thank Dr. Damir  
553 Kronic from the DKFZ light microscopy facility for his assistance in image analysis. The DKFZ flow  
554 cytometry, light microscopy, genomics and proteomics, and laboratory animal core facilities are  
555 gratefully acknowledged for their excellent support. This work was supported by grants from the  
556 Deutsche Forschungsgemeinschaft [project FE 1282/2-1 to M. Felcht]; DFG-funded Research Training  
557 Group 2099 “Hallmarks of Skin Cancer” [project number 259332240 to H.G. Augustin, M. Felcht, C.  
558 Géraud, S. Goerdts and J. Utikal]; the DFG-funded Collaborative Research Center CRC-TR209  
559 “Hepatocellular Carcinoma” [project C3 to S. Goerdts and H. G. Augustin], and the European Research  
560 Council Advanced Grant “AngioMature” [project 787181 to H. G. Augustin].

561 **References**

- 562 1. Siegel RL, Miller KD, Jemal A. Cancer statistics, 2019. *CA Cancer J Clin* **2019**;69:7-34
- 563 2. Schadendorf D, Fisher DE, Garbe C, Gershenwald JE, Grob JJ, Halpern A, *et al.* Melanoma. *Nat Rev*  
564 *Dis Primers* **2015**;1:15003
- 565 3. Gide TN, Wilmott JS, Scolyer RA, Long GV. Primary and acquired resistance to immune checkpoint  
566 inhibitors in metastatic melanoma. *Clin Cancer Res* **2018**;24:1260-70
- 567 4. Schadendorf D, van Akkooi ACJ, Berking C, Griewank KG, Gutzmer R, Hauschild A, *et al.* Melanoma.  
568 *Lancet* **2018**;392:971-84
- 569 5. Saharinen P, Eklund L, Alitalo K. Therapeutic targeting of the angiopoietin-TIE pathway. *Nat Rev Drug*  
570 *Discov* **2017**;16:635-61
- 571 6. Nasarre P, Thomas M, Kruse K, Helfrich I, Wolter V, Deppermann C, *et al.* Host-derived angiopoietin-  
572 2 affects early stages of tumor development and vessel maturation but is dispensable for later  
573 stages of tumor growth. *Cancer Res* **2009**;69:1324-33
- 574 7. Srivastava K, Hu J, Korn C, Savant S, Teichert M, Kapel SS, *et al.* Postsurgical adjuvant tumor therapy  
575 by combining anti-angiopoietin-2 and metronomic chemotherapy limits metastatic growth. *Cancer*  
576 *Cell* **2014**;26:880-95
- 577 8. Helfrich I, Edler L, Sucker A, Thomas M, Christian S, Schadendorf D, *et al.* Angiopoietin-2 levels are  
578 associated with disease progression in metastatic malignant melanoma. *Clin Cancer Res*  
579 **2009**;15:1384-92
- 580 9. Augustin HG, Koh GY, Thurston G, Alitalo K. Control of vascular morphogenesis and homeostasis  
581 through the angiopoietin-Tie system. *Nat Rev Mol Cell Biol* **2009**;10:165-77
- 582 10. Sfiligoi C, de Luca A, Cascone I, Sorbello V, Fuso L, Ponzzone R, *et al.* Angiopoietin-2 expression in  
583 breast cancer correlates with lymph node invasion and short survival. *Int J Cancer* **2003**;103:466-74
- 584 11. Gu J, Yamamoto H, Ogawa M, Ngan CY, Danno K, Hemmi H, *et al.* Hypoxia-induced up-regulation of  
585 angiopoietin-2 in colorectal cancer. *Oncol Rep* **2006**;15:779-83
- 586 12. Maffei R, Martinelli S, Castelli I, Santachiara R, Zucchini P, Fontana M, *et al.* Increased angiogenesis  
587 induced by chronic lymphocytic leukemia B cells is mediated by leukemia-derived Ang2 and VEGF.  
588 *Leuk Res* **2010**;34:312-21
- 589 13. Iwamoto T, Takahashi M, Ito M, Hamatani K, Ohbayashi M, Wajjwalku W, *et al.* Aberrant  
590 melanogenesis and melanocytic tumour development in transgenic mice that carry a  
591 metallothionein/ret fusion gene. *EMBO J* **1991**;10:3167-75

- 592 14. Teichert M, Stumpf C, Booken N, Wobser M, Nashan D, Hallermann C, *et al.* Aggressive primary  
593 cutaneous B-cell lymphomas show increased Angiopoietin-2-induced angiogenesis. *Exp Dermatol*  
594 **2015**;24:424-9
- 595 15. Schmittnaegel M, Rigamonti N, Kadioglu E, Cassara A, Wyser Rmili C, Kiialainen A, *et al.* Dual  
596 angiopoietin-2 and VEGFA inhibition elicits antitumor immunity that is enhanced by PD-1 checkpoint  
597 blockade. *Sci Transl Med* **2017**;9
- 598 16. Loboda A, Damulewicz M, Pyza E, Jozkowicz A, Dulak J. Role of Nrf2/HO-1 system in development,  
599 oxidative stress response and diseases: an evolutionarily conserved mechanism. *Cell Mol Life Sci*  
600 **2016**;73:3221-47
- 601 17. Petrova V, Annicchiarico-Petruzzelli M, Melino G, Amelio I. The hypoxic tumour microenvironment.  
602 *Oncogenesis* **2018**;7:10
- 603 18. Cogliati S, Enriquez JA, Scorrano L. Mitochondrial cristae: Where beauty meets functionality. *Trends*  
604 *Biochem Sci* **2016**;41:261-73
- 605 19. Fuhrmann DC, Brune B. Mitochondrial composition and function under the control of hypoxia.  
606 *Redox Biol* **2017**;12:208-15
- 607 20. Fu W, Liu Y, Yin H. Mitochondrial dynamics: Biogenesis, fission, fusion, and mitophagy in the  
608 regulation of stem cell behaviors. *Stem Cells Int* **2019**;2019:9757201
- 609 21. Favaro G, Romanello V, Varanita T, Andrea Desbats M, Morbidoni V, Tezze C, *et al.* DRP1-mediated  
610 mitochondrial shape controls calcium homeostasis and muscle mass. *Nat Commun* **2019**;10:2576
- 611 22. Divakaruni AS, Brand MD. The regulation and physiology of mitochondrial proton leak. *Physiology*  
612 (Bethesda) **2011**;26:192-205
- 613 23. Zhang J, Wang X, Vikash V, Ye Q, Wu D, Liu Y, *et al.* ROS and ROS-mediated cellular signaling. *Oxid*  
614 *Med Cell Longev* **2016**;2016:4350965
- 615 24. Rigamonti N, Kadioglu E, Keklikoglou I, Wyser Rmili C, Leow CC, De Palma M. Role of angiopoietin-2  
616 in adaptive tumor resistance to VEGF signaling blockade. *Cell Rep* **2014**;8:696-706
- 617 25. Fiedler U, Scharpfenecker M, Koidl S, Hegen A, Grunow V, Schmidt JM, *et al.* The Tie-2 ligand  
618 angiopoietin-2 is stored in and rapidly released upon stimulation from endothelial cell Weibel-  
619 Palade bodies. *Blood* **2004**;103:4150-6
- 620 26. Oliner J, Min H, Leal J, Yu D, Rao S, You E, *et al.* Suppression of angiogenesis and tumor growth by  
621 selective inhibition of angiopoietin-2. *Cancer Cell* **2004**;6:507-16

- 622 27. Imanishi Y, Hu B, Jarzynka MJ, Guo P, Elishaev E, Bar-Joseph I, *et al.* Angiopoietin-2 stimulates breast  
623 cancer metastasis through the alpha(5)beta(1) integrin-mediated pathway. *Cancer Res*  
624 **2007**;67:4254-63
- 625 28. Hu B, Guo P, Fang Q, Tao HQ, Wang D, Nagane M, *et al.* Angiopoietin-2 induces human glioma  
626 invasion through the activation of matrix metalloprotease-2. *Proc Natl Acad Sci U S A*  
627 **2003**;100:8904-9
- 628 29. Moriya H. Quantitative nature of overexpression experiments. *Mol Biol Cell* **2015**;26:3932-9
- 629 30. De Palma M, Biziato D, Petrova TV. Microenvironmental regulation of tumour angiogenesis. *Nat Rev*  
630 *Cancer* **2017**;17:457-74
- 631 31. Li T, Liu Z, Jiang K, Ruan Q. Angiopoietin2 enhances doxorubin resistance in HepG2 cells by  
632 upregulating survivin and Ref-1 via MSK1 activation. *Cancer Lett* **2013**;337:276-84
- 633 32. Schulz P, Fischer C, Detjen KM, Rieke S, Hilfenhaus G, von Marschall Z, *et al.* Angiopoietin-2 drives  
634 lymphatic metastasis of pancreatic cancer. *FASEB J* **2011**;25:3325-35
- 635

## Figure legends

**Figure 1. Melanoma cells express ANGPT2.** (A) Immunohistochemical analysis of ANGPT2 expression in tissue biopsies of human melanomas. Scale bar: 100 $\mu$ M. (B) Tissue sections from melanoma patients were stained with *ANGPT2* RNASCOPE probe. Square boxes depict regions of interest (ROIs) at a higher magnification. Scale bar: 50 $\mu$ M. (C) Quantitation of the number of patients with detectable expression of ANGPT2 in tumor cells of benign melanocytic nevi (n=8), primary (n=33), and metastatic melanomas (n=92). \*, p<0.05, Chi-square test. (D) *Angpt2* and *Tek* expression were quantified using qRT-PCR in mouse melanoma cell lines and mouse lung EC (ND= non-detected). (E) ANGPT2 ELISA was performed to quantify ANGPT2 protein in supernatants of control and *Angpt2* knockdown cells (sh-1 and sh-2) in RET and B16F10n=3; mean  $\pm$  SD). \*, p<0.05, \*\*, p<0.01, two-tailed unpaired Student's t-test.

**Figure 2. *Angpt2* knockdown in tumor cells does not alter primary tumor growth.** (A) Tumor weight at day 14 after primary tumor inoculation of control RET and knockdown cell lines (n=12; mean  $\pm$  SD). (B) *Angpt2* expression in control and *Angpt2* knockdown RET primary tumors quantified by qRT-PCR (n=8-9; mean  $\pm$  SD). \*, p<0.05, \*\*\*\*, p<0.0001, Mann Whitney U test. (C) On the left, representative H&E images of control and *Angpt2* knockdown RET primary tumors are shown. Arrowheads indicate necrotic area. Scale bar: 1mm. On the right, quantitation of necrotic area is shown (n=9-11 mean  $\pm$  SD). \*, p<0.05, Mann Whitney U test. (D) On the left, representative images of tumor sections stained with KI67 (in red). Scale bar: 200 $\mu$ m. On the right, quantitation of KI67-positive area normalized to DAPI area in control and *Angpt2* knockdown RET primary tumors (n=5-6; mean  $\pm$  SD). (E) ANGPT2 ELISA was performed to quantify ANGPT2 protein levels in supernatants of control+Plenti, sh-2+Plenti and sh-2+Plenti *Angpt2* cells in RET (n=3; mean  $\pm$  SD). \*, p<0.05, \*\*, p<0.01, two-tailed unpaired Student's t-test. (F) On the left, representative H&E images of control+Plenti, sh-2+Plenti and sh-2+Plenti *Angpt2* RET primary tumors are shown. Arrowheads indicate necrotic area. Scale bar: 1mm. On the right, quantitation of necrotic area is shown (n=6 mean  $\pm$  SD). \*, p<0.05, Mann Whitney U test.

**Figure 3. *Angpt2* knockdown in tumor cells does not impact immune cell infiltration.** (A-B) FACS-based immune analysis was performed control and *Angpt2* knockdown RET primary tumors on day 14 after tumor implantation. Shown are the quantitation of tumor infiltrating lymphoid (A) and myeloid cells (B) (n=9-11; mean  $\pm$  SD). All comparisons were rendered non-significant by Mann Whitney U test.

**Figure 4. Tumor cell-expressed *Angpt2* modulates ROS and mitochondrial homeostasis.** (A) On the left, heatmap depicting differentially regulated genes between control- and *Angpt2*-silenced tumor cells. On the right, gene set enrichment analysis identifying alterations in pathways involved in maintaining

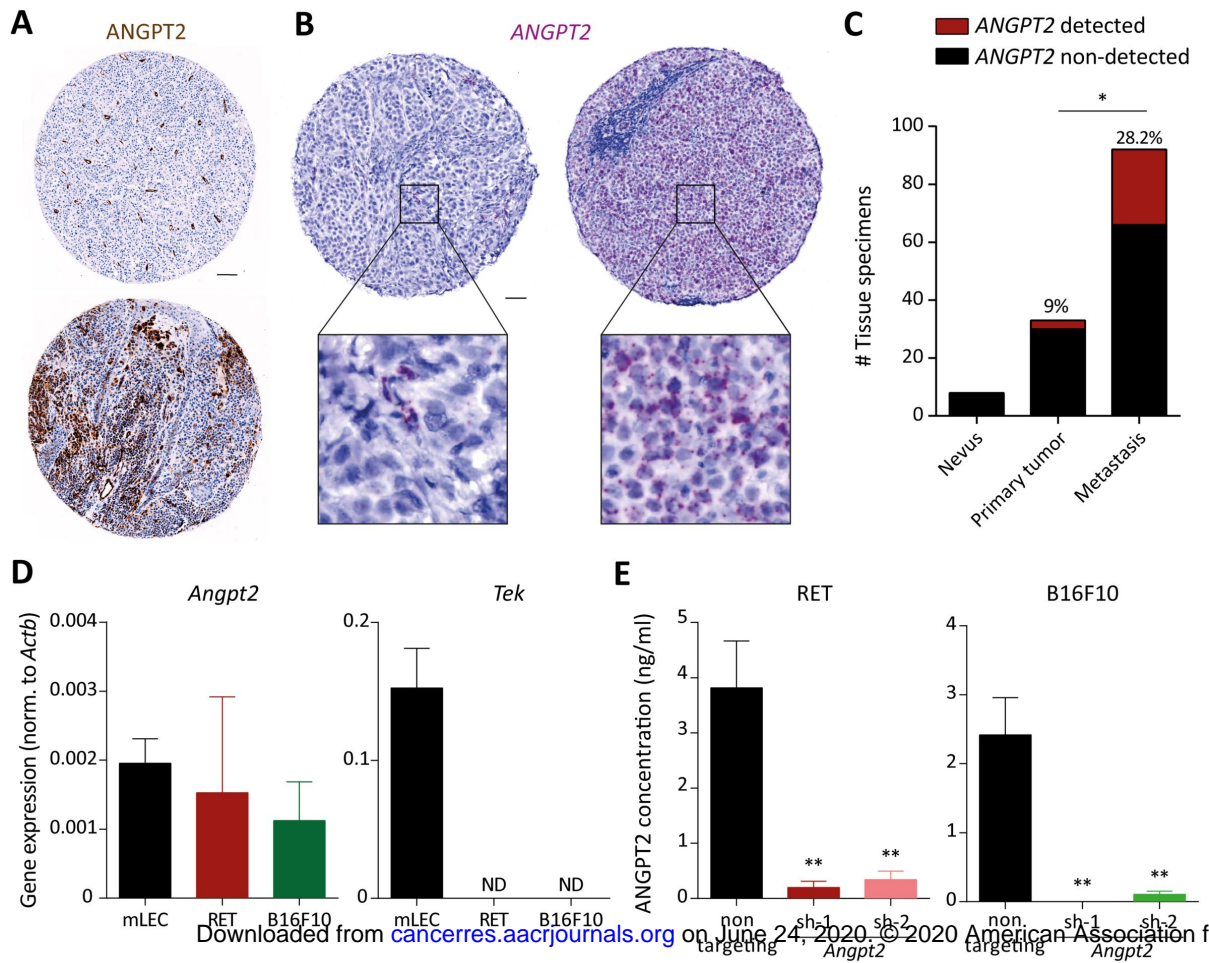


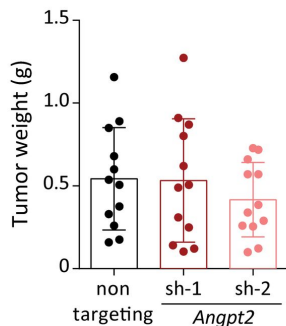
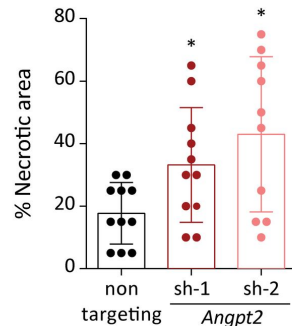
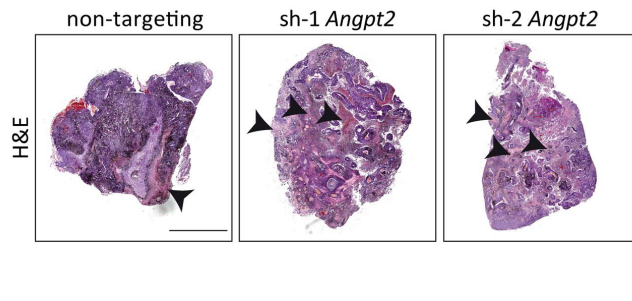
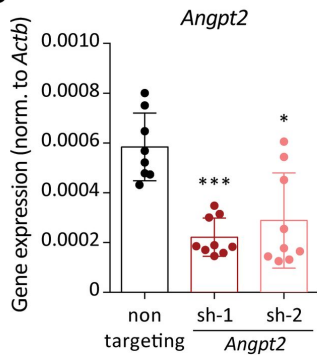
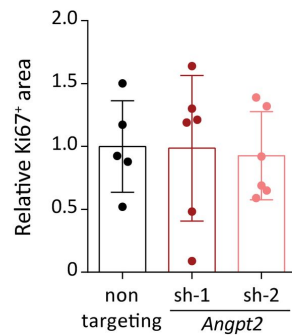
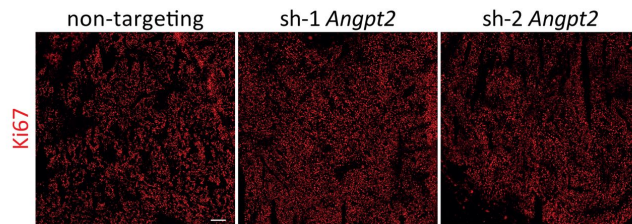
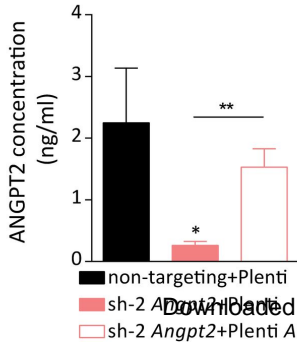
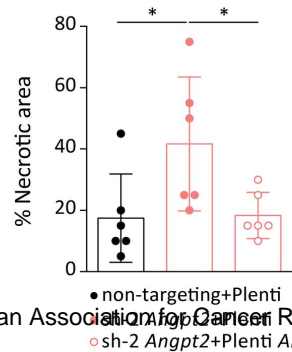
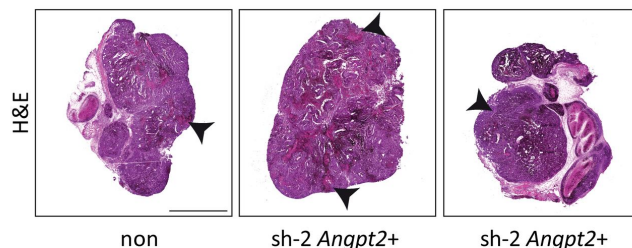
oxidative homeostasis (NES=normalized enrichment score). **(B)** Spearman correlation analysis of *ANGPT2*, *NFE2L2*, and *HMOX1* in cutaneous melanoma (SKCM) dataset from TCGA database. **(C)** *Hmox1* expression in control and *Angpt2* knockdown RET primary tumors was quantified using qRT-PCR (n=8-9; mean  $\pm$  SD). \*, p<0.05, Mann Whitney U test. **(D)** FACS analysis of ROS levels in control and *Angpt2* knockdown RET primary tumors (n=4-5; mean  $\pm$  SD). \*, p<0.05, Mann Whitney U test. **(E)** Representative electron microscopic images depicting morphological changes in mitochondria of wild type and *Angpt2*-silenced RET tumor cells. Cells were kept under 1% O<sub>2</sub> and serum starvation condition for 24h before processing for electron microscopy. Square boxes depict ROIs at higher magnification. Scale bar: 2 $\mu$ m. **(F)** Quantitation of fragmented mitochondria per cell (n=16-19 cells/condition; mean  $\pm$  SD). \*, p<0.05, Mann Whitney U test. **(G)** Proton leak in control and *Angpt2* knockdown RET tumor cells was measured in a Seahorse Mito Stress experiment. Prior to Seahorse analysis, cells were kept under 1% O<sub>2</sub> for 6h (n=5; mean  $\pm$  SD). \*p<0.05, \*\*p<0.01, two-tailed paired Student's t-test. **(H)** Western blot analysis was performed for phospho-ERK, phospho-P38, total-P38, and total-ERK in control and *Angpt2* knockdown RET primary tumors. Actin was used as a loading control (n=6).

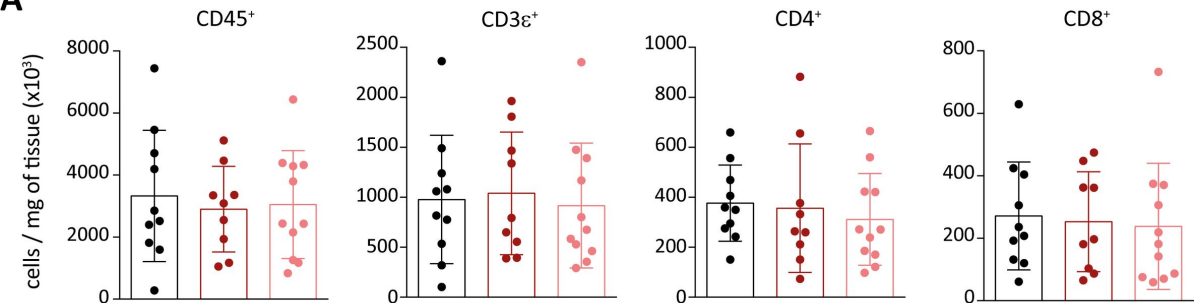
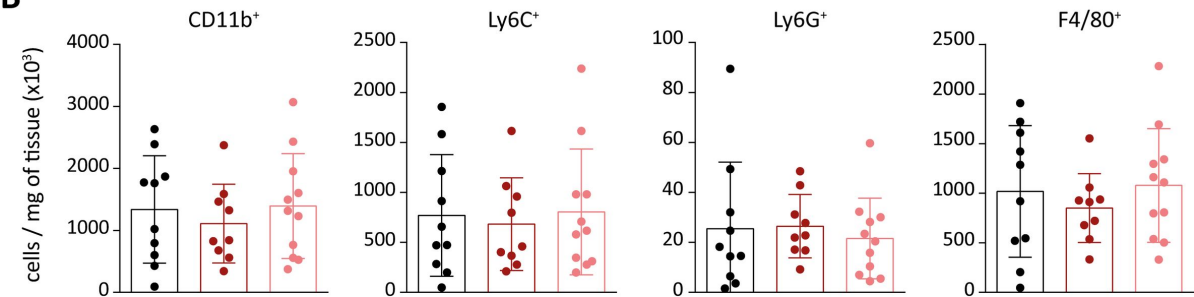
**Figure 5. Tumor cell-expressed *Angpt2* promotes metastasis.** **(A)** Control or *Angpt2*-deficient RET cells were injected into the tail vein of C57BL/6N mice. Mice were sacrificed after 14 days. Shown are the representative images of lung metastatic foci imaged under a stereomicroscope. Scale bar: 5mm. **(B)** The graph represents the quantitation of lung metastatic foci (n=9; mean  $\pm$  SD). \*, p<0.05, \*\*, p<0.01, Mann Whitney U test. **(C)** Control (in red) and *Angpt2*-silenced (in green) RET tumor cells were co-injected intravenously in mice. Lungs were harvested 14 days after tumor cell inoculation and visualized under a fluorescent dissection microscope. Representative images of lung metastatic foci are shown. Scale bar: 2mm. **(D)** Quantitation of lung colonization by control (in red) or *Angpt2*-silenced (in green) RET tumor cells. The area of each metastatic colony (RFP/GFP) was normalized to the combined fluorescent area (n=5-6; mean  $\pm$  SD). **(E)** Control+Plenti, sh-2+Plenti and sh-2+Plenti *Angpt2* cells were injected into the tail vein of C57BL/6N mice. Mice were sacrificed after 14 days. Shown are representative images of lung metastatic foci imaged under a stereomicroscope. Scale bar: 5mm. **(F)** The graph represents the quantitation of lung metastatic foci (n=6; mean  $\pm$  SD). \*\*, p<0.01, Mann Whitney U test. **(G)** WT C57BL/6N mice were intradermally injected with either 300,000 control or *Angpt2* knockdown RET tumor cells in the ear and regional LN were collected 2 weeks later. Representative H&E images of LN. Arrowheads indicate detectable metastases. **(H)** The incidence of LN metastasis is depicted (n=6).

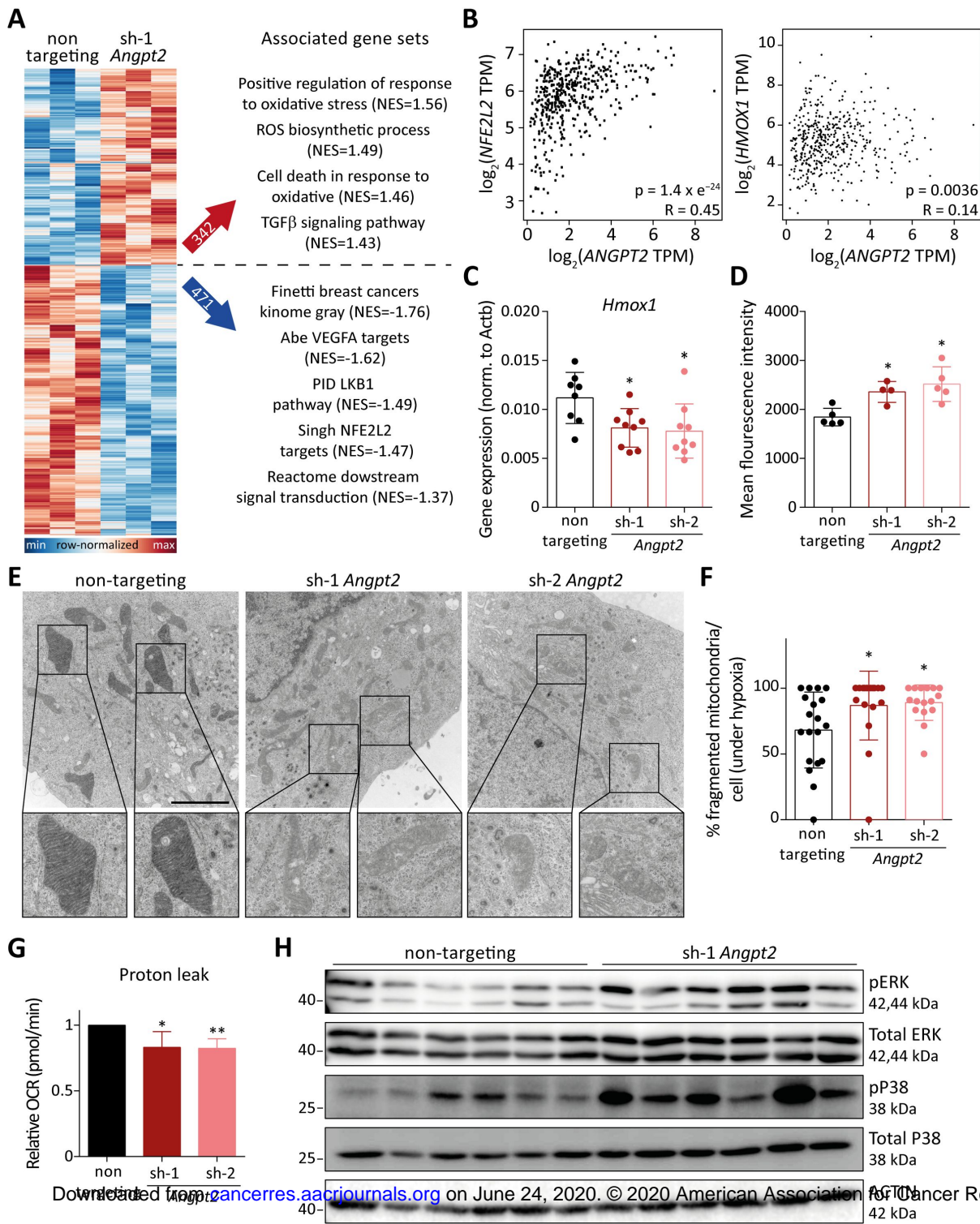
**Figure 6. Administration of NAC rescues metastasis. (A)** Schematic illustration of the rescue experiment to investigate the influence of ROS on regulating tumor cell-*Angpt2* mediated metastasis. **(B)** Control or *Angpt2*-deficient RET cells were injected into the tail vein of C57BL/6N mice. Mice were administered either regular water or water containing 1g/l NAC. Mice were sacrificed after 14 days. Shown are the representative images of lung metastatic foci imaged under a stereomicroscope. Scale bar: 5mm. **(C)** The graph represents the quantitation of lung metastatic foci (n=12; mean  $\pm$  SD). \*, p<0.05, \*\*, p<0.01, Mann Whitney U test.

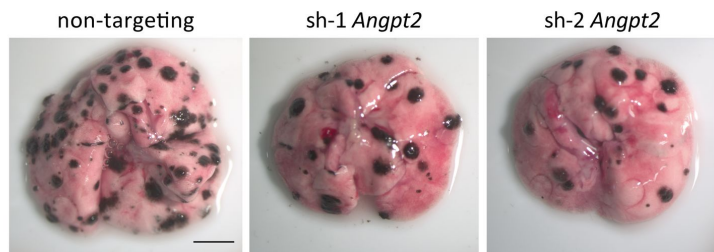
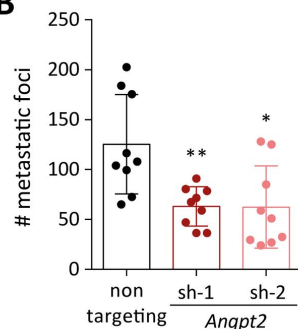
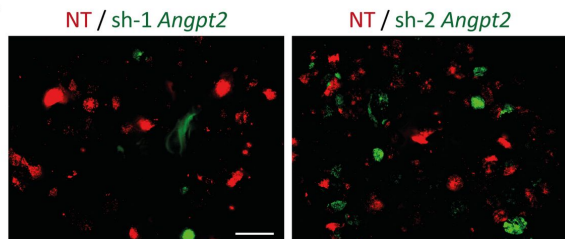
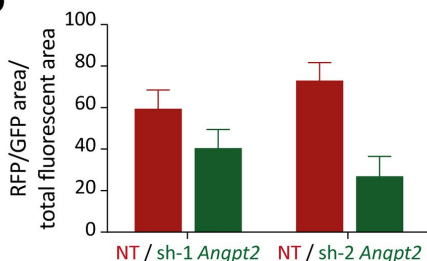
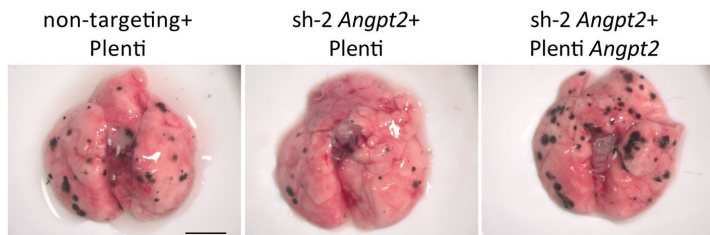
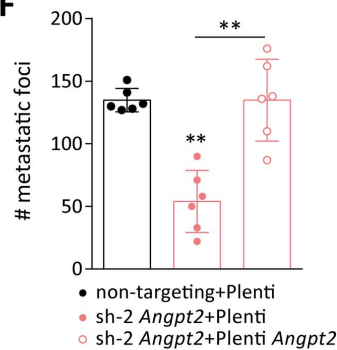
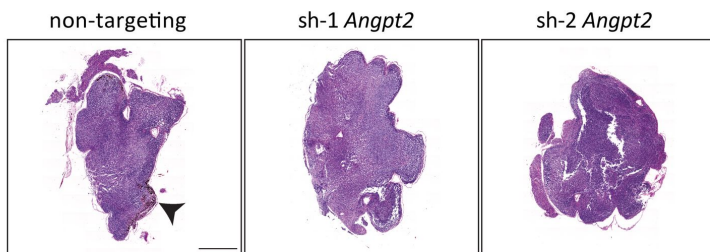
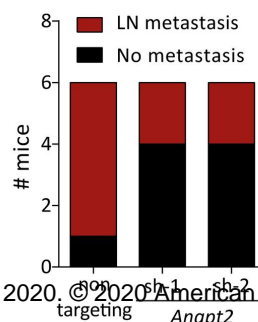
# Figure 1



**Figure 2****A****C****B****D****E****F**

**Figure 3****A****B**

**Figure 4**

**Figure 5****A****B****C****D****E****F****G****H**

**Figure 6**

**A**

NAC (1 g/l) in drinking water



Administration of  
NAC in drinking water (d0)



i.v. injection of  
Tumor cells (d1)

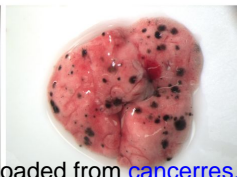
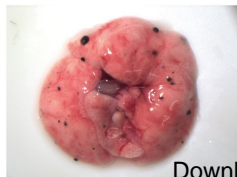
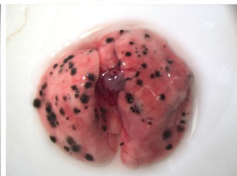


Lung analysis  
(d15)

**B**

non-targeting

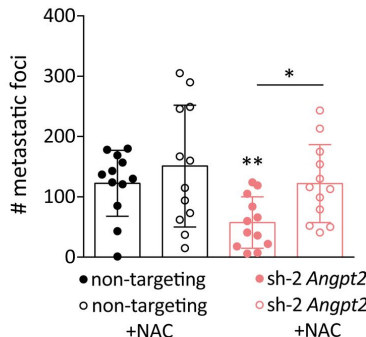
non-targeting+NAC



sh-2 *Angpt2*

sh-2 *Angpt2*+NAC

**C**





# Cancer Research

The Journal of Cancer Research (1916–1930) | The American Journal of Cancer (1931–1940)

## Tumor cell-derived Angiopoietin-2 promotes metastasis in melanoma

Ashik Ahmed Abdul Pari, Mahak Singhal, Corinne Hübers, et al.

*Cancer Res* Published OnlineFirst April 17, 2020.

<b>Updated version</b>	Access the most recent version of this article at: doi: <a href="https://doi.org/10.1158/0008-5472.CAN-19-2660">10.1158/0008-5472.CAN-19-2660</a>
<b>Supplementary Material</b>	Access the most recent supplemental material at: <a href="http://cancerres.aacrjournals.org/content/suppl/2020/04/17/0008-5472.CAN-19-2660.DC1">http://cancerres.aacrjournals.org/content/suppl/2020/04/17/0008-5472.CAN-19-2660.DC1</a>
<b>Author Manuscript</b>	Author manuscripts have been peer reviewed and accepted for publication but have not yet been edited.

**E-mail alerts** [Sign up to receive free email-alerts](#) related to this article or journal.

**Reprints and Subscriptions** To order reprints of this article or to subscribe to the journal, contact the AACR Publications Department at [pubs@aacr.org](mailto:pubs@aacr.org).

**Permissions** To request permission to re-use all or part of this article, use this link <http://cancerres.aacrjournals.org/content/early/2020/04/17/0008-5472.CAN-19-2660>. Click on "Request Permissions" which will take you to the Copyright Clearance Center's (CCC) Rightslink site.